nzsee
NEW ZEALAND SOCIETY FOR EARTHQUAKE ENGINEERING

Towards 3D ground motion simulation-based site amplification: a Wellington, New Zealand, case study considering multiple basin geometries

R. L. Lee, B.A. Bradley & C. de la Torre
University of Canterbury, Christchurch, New Zealand.

M.P. Hill & A.E. Kaiser
GNS Science Te Pu Ao, Lower Hutt, New Zealand.

L.M. Wotherspoon
University of Auckland, Auckland, New Zealand.

ABSTRACT

This paper presents a study on 3D ground motion simulation-based site amplification using the Wellington region of New Zealand as a case study. Several recent models of the Wellington sedimentary basin have been developed and are used in the simulations conducted as a part of this study to investigate the influence of basin geometry on site amplification. Location-specific site amplification factors for acceleration response spectra are presented at key locations throughout the Wellington CBD to illustrate how the simulated site amplification compare with observations. The simulations are found to produce amplification factors that have comparable level of amplification to observed amplification factors at deeper basin locations. Several limitations are also highlighted in this comparison. At shallow basin locations, the spatial resolution of the simulations conducted are not able to properly capture the basin response. Due to an enforced minimum S-wave velocity of 500 m/s in the simulations, the periods of spectral peaks are not accurately matched between simulation and observation. This provides motivation for further research into improvement and advancements in the simulations.

1 INTRODUCTION

The Wellington region of New Zealand (NZ) is built upon a complex sedimentary basin that has been observed to amplify earthquake ground motions from historical events, such as the 2016 Mw 7.8 Kaikōura earthquake (Bradley et al. 2018). Accurate modelling of such basin effects would lead to improved seismic hazard modelling.

This paper presents progress towards modelling of site amplification caused by basin effects using 3D physics-based ground motion simulations. The Wellington CBD is the focus of this paper given that it is a major urban area, the capital of NZ and exposed to high seismic hazard. Several basin geometries are considered in the simulations to understand the predicted amplification resulting from alternative models. Comparisons of response spectral amplification at key locations are provided to illustrate the sensitivity of the site amplification to alternative basin models and to quantify the performance of the simulations against observed ground motions where available.

2 WELLINGTON BASIN MODELS

This study considers seven recently developed sedimentary basin models of the Wellington region, primarily from two studies. The Stronach and Stern (2021) suite of models are considered here, with shallow, preferred and deep representations of the basin to account for different inferences and uncertainty in the adopted data and modelling. The models will herein be referred to as S21 Shal, S21 Pref and S21 Deep, respectively. The Hill et al. (2022) suite of models developed as a part of the 2022 NZ National Seismic Hazard Model (NSHM) Revision are also included. The Hill et al. (2022) study also has shallow, preferred and deep representations and will herein be referred to as H22 Shal, H22 Pref and H22 Deep, respectively. An interim model obtained during the development of the Hill et al. (2022) models is also considered in this study as an alternative model and will herein be referred to as H21.

Basin elevation plots for the considered models are presented in Figure 1 for the Wellington CBD. Important areas and regional features are indicated in Figure 1a. Beneath most of the CBD, the depth of the sedimentary basin is relatively shallow, on the order of 0-200 m. Deeper locations within the basin tend to range from 300-600 m but are mostly at the coastline or offshore in the harbour.

3 OBSERVED EARTHQUAKE AND GROUND MOTION DATA

Six earthquakes are considered in this study, ranging from Mw 5.5-6.6. The locations of the earthquakes are shown in Figure 2. Centroid moment tensor solutions were obtained from GeoNet and converted to finite fault geometries using Leonard (2010) Mw-scaling relationships.

Observed ground motion data was obtained from the GeoNet FDSN server as a part of the 2022 NZ NSHM Revision ground-motion database (Hutchinson et al. 2022) with an additional low-pass filter applied to retain only low frequencies ($f \leq 2.5$ Hz) to allow for a more consistent comparison with the simulations conducted which only contain low frequency content.

4 GROUND-MOTION SIMULATION METHOD AND COMPUTATION DETAILS

This study adopts the low-frequency (LF) component of the commonly used Graves and Pitarka (2016) hybrid broadband ground-motion simulation method. Only the LF component is used (and not the high-frequency component) because the 3D Wellington sedimentary basin is only explicitly modelled in the LF crustal velocity model. This is a finite difference approach with 4th-order spatial and 2nd-order temporal accuracies.

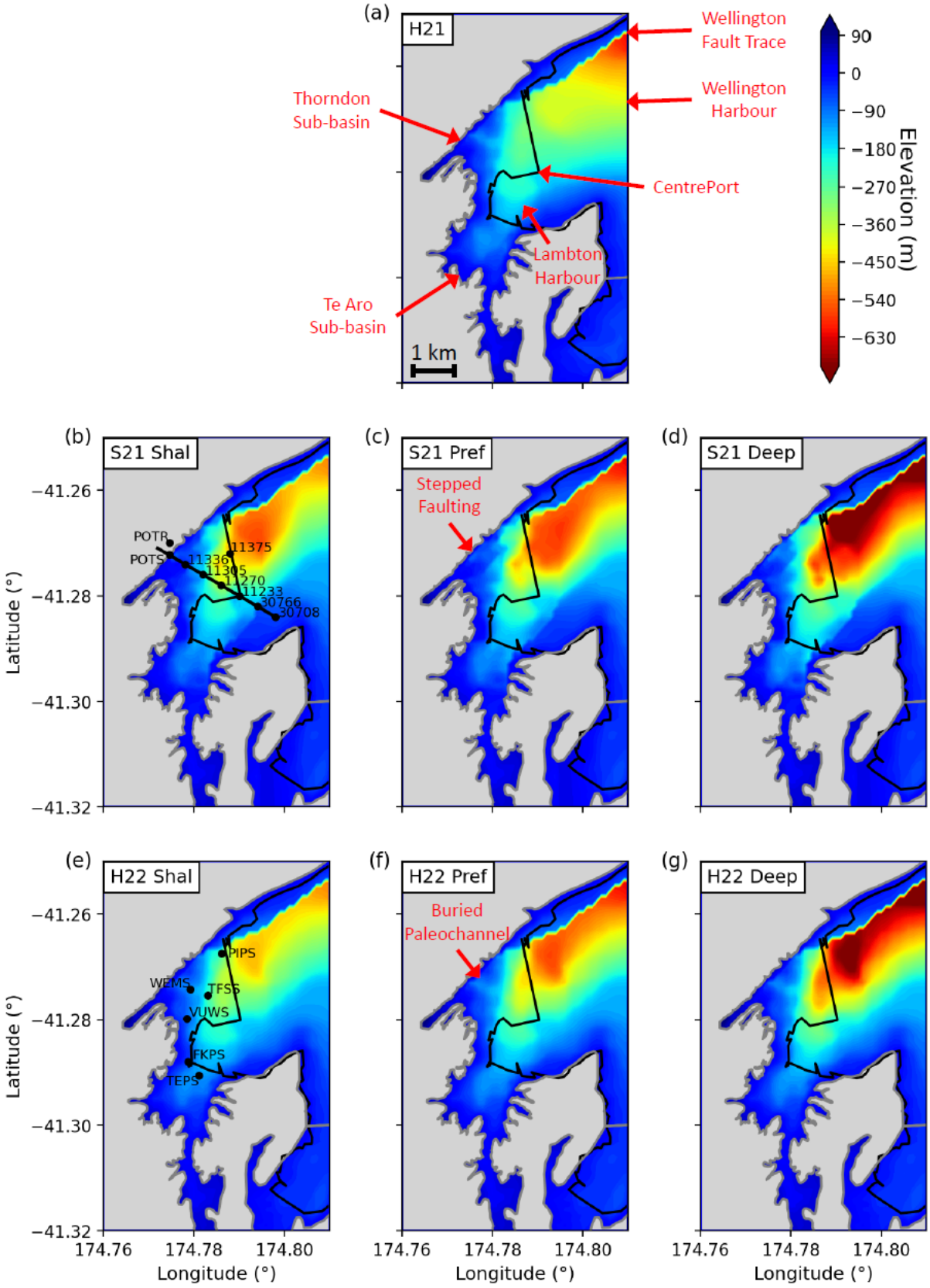

Figure 1: Elevation plots of Wellington sedimentary basin models used in ground-motion simulations this study across the Wellington CBD: (a) H21, (b) S21 Shal, (c) S21 Pref, (d) S21 Deep, (e) H22 Shal, (f) H22 Pref, (g) H22 Deep. The black line indicates the coastline and grey shaded areas indicate regions outside of the sedimentary basin (e.g. outcropping rock).

4.1 Crustal Velocity Model

The NZ Velocity Model (NZVM; Thomson et al. 2019) is used with the different sedimentary basin models to generate crustal velocity models used in the simulations. The velocity models comprise embedded sedimentary basin models within a background travel-time tomography model, with a geotechnical layer applied to the top 350 m of the travel-time tomography model to better model surficial soil and weathered rock conditions.

4.2 Kinematic Rupture Models

Kinematic rupture models for each earthquake are generated using the Graves and Pitarka (2016) kinematic rupture generator which produces spatially-correlated distributions of slip amplitude, slip temporal evolution, rise time and rake angle across the finite fault. The hypocenter location is set at the center of the finite fault. While this assumption is not precise, it is considered adequate in the absence of explicit data and with the coarse layer thickness in the 1D velocity model used in the generation of kinematic rupture parameters.

4.3 Simulation Input and Computational Details

The horizontal extent of the simulation domain is shown in the Figure 2 inset. A minimum S-wave velocity of 500 m/s is enforced with 50 m spatial grid spacing. This results in a maximum resolvable frequency of 2.0 Hz. The simulations are run with a time step of 0.0025 s.

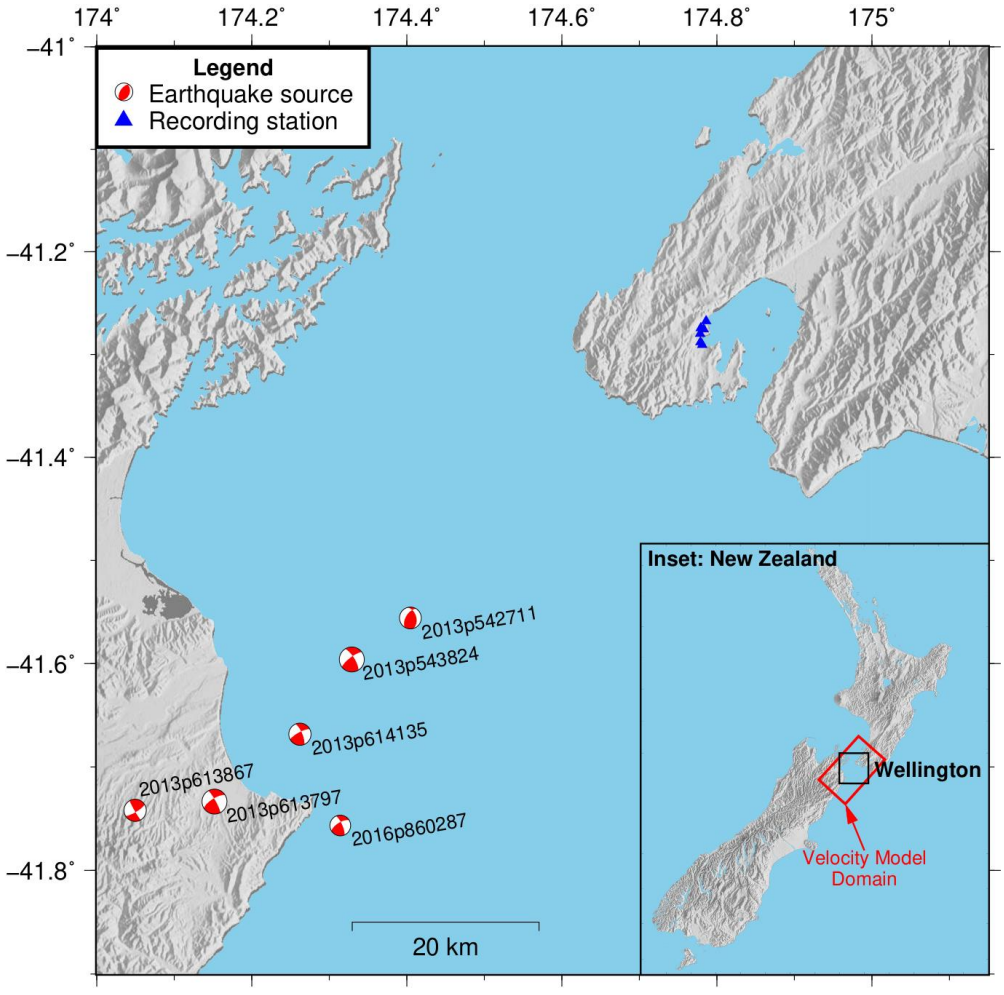

Figure 2: Map showing the locations of 6 earthquake sources and ground-motion recording stations considered in this study. The horizontal domain for crustal velocity models used in simulations are shown as the red box in the inset.

5 SITE AMPLIFICATION FROM 3D SIMULATIONS

The site amplification factor in this study is defined:

$$Amp_{s,m,e}(T) = \frac{SA_{s,m,e}(T)}{SA_{r,m,e}(T)} \quad (1)$$

Where $SA_{s,m,e}(T)$ and $SA_{r,m,e}(T)$ are the response spectral ordinates for vibration period T at the site of interest s and reference site r, respectively, for a basin model m and event e. POTS is used as the reference site for observed site amplification factors, while an artificial location slightly north of POTS on rock named POTR is used as the reference site for simulated site amplification factors. POTS is used for the observed reference station because it has been found to have flat response over the frequency range of interest (Bradley et al. 2018). POTS has a measured V_{s30} of 453 m/s. POTR is used for the simulated site amplification factors because the reference velocity at POTS in the simulation changes depending on the basin model used. In the simulations, POTR has a V_{s30} of 1173 m/s. Since the reference conditions are different between observation and simulation (as well the site conditions themselves), this study is essentially seeking to compare the simulated site amplification factors as-is (i.e. how they are produced in the simulations) against observed site amplification factors, which is consistent with previous studies of this nature.

Figures 3 and 4 present location-specific spectral amplification factors at artificial and real ground-motion recording station locations. Within each plot, the event-averaged amplification (i.e. across the six earthquakes) for each basin model is shown as the thick lines (solid or dashed), the red-shaded area indicates the +/-1 standard deviation of the S21 Pref model, and the grey-shaded area indicates the +/-1 standard deviation of observed amplification factors where applicable. Plot legends also include the modelled depth to basin boundary at each location for each basin model.

Figure 3 presents simulated spectral amplification factors at eight locations: POTS, 11375 (artificial station) and six artificial stations along a NW-SE transect shown in Figure 1b. The small amplification at POTS relative to POTR (Fig. 3a) indicates that spectral acceleration amplitudes are typically similar between the two locations. 11336 and 30708 (Fig. 3c and 3h) show relatively large differences between S21 basin models, and H21 or H22 models. This is primarily due to the different number of finite difference nodes representing the basin beneath and adjacent to the site. The first node is located at 25 m below the ground surface (half the grid spacing) and second node is at 75 m. For H21 and H22 models, there is at most 1 finite difference node immediately beneath the site (sometimes none) while the S21 models have at least 2 finite difference grid points and hence the latter is better able to resolve the basin response. These highlight limitations caused by the spatial resolution of the simulations at shallow basin sites. At other artificial station locations shown (Fig. 3b-3g), the site amplification factors are relatively similar between basin models although with some period-dependent differences. At 11375 (Fig. 3b) corresponding to the deepest onshore location, the H21 model appears to have the most difference relative to other models, with a narrower peak and more rapid drop off at longer periods.

Figure 4 presents observed and simulated spectral amplification factors at six real ground motion recording stations: WEMS, PIPS, VUWS, TFSS in the Thorndon sub-basin; and FKPS and TEPS in the Te Aro sub-basin. The locations of these stations are shown in Figure 1b. Limitations with the spatial resolution noted earlier are evident at locations VUWS and FKPS for all basin models, and for the H21 and H22 models at WEMS. At PIPS and TFSS, which are deeper sites, amplification factors are larger across a broader range of vibration periods in the simulations and align relatively well with observations. The level of amplification is comparable between observation and simulation at these sites. Lastly, TEPS has very large observed and simulated amplification factors at the periods corresponding to their respective spectral peaks. However, the observed and simulated spectral peak periods differ, at approximately T = 0.7 s for simulated and T = 1.1 s for

observed. This difference is likely due to the minimum S-wave velocity of 500 m/s enforced in the simulation which causes the spectral peak to occur at a shorter period compared to the softer soil conditions in reality.

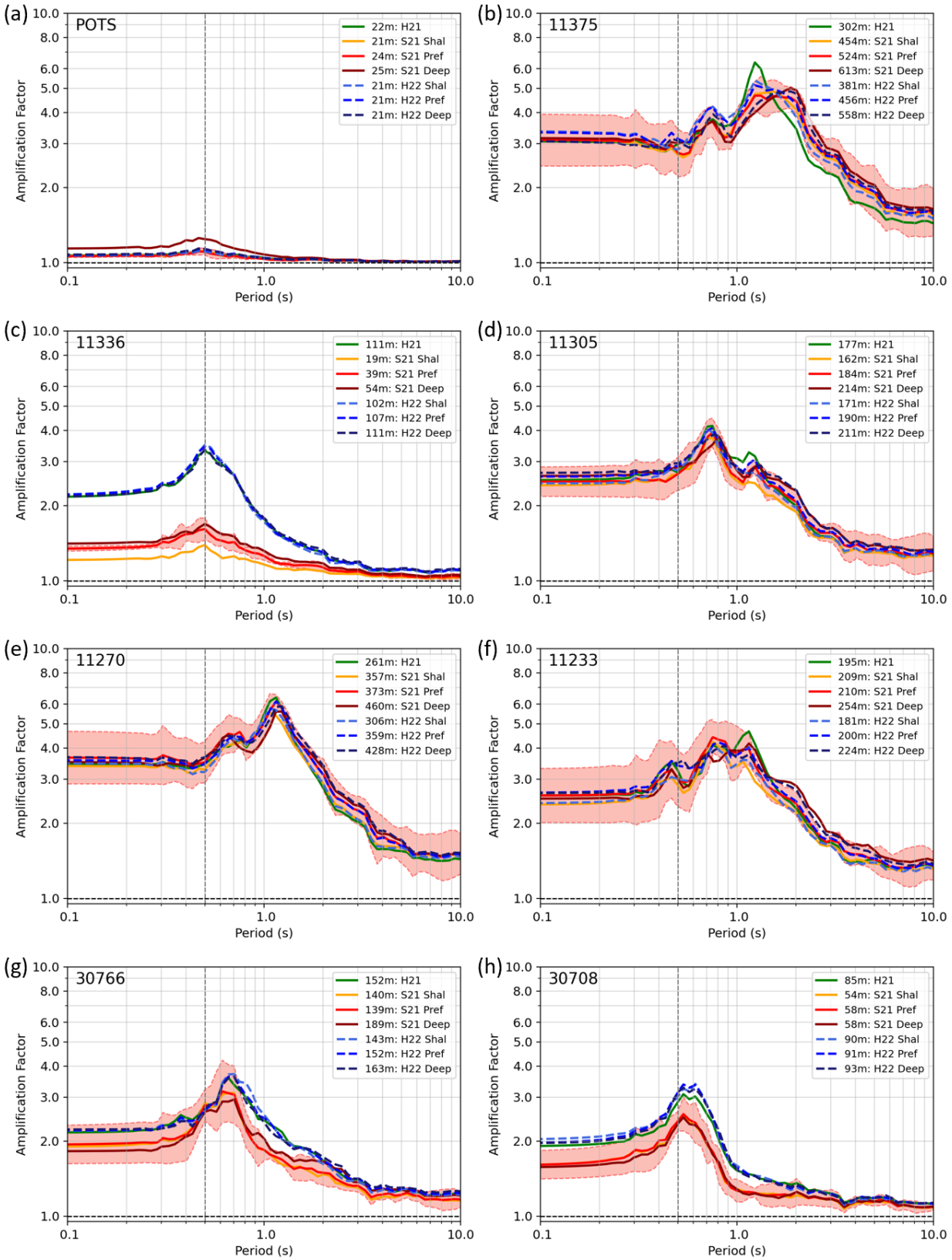

Figure 3: Simulated site amplification factors for each basin model averaged across the 6 earthquakes for locations: (a) POTS, (b) 11375, (c) 11336, (d) 11305, (e) 11270, (f) 11233, (g) 30766, and (h) 30708. The

red-shaded area indicates the +/-1 standard deviation of the S21 Pref model. Simulated standard deviations are similar between basin models and therefore others are not plotted to reduce visual clutter. The vertical dashed line indicates T = 0.5 s which is the minimum reliable period of the LF simulations.

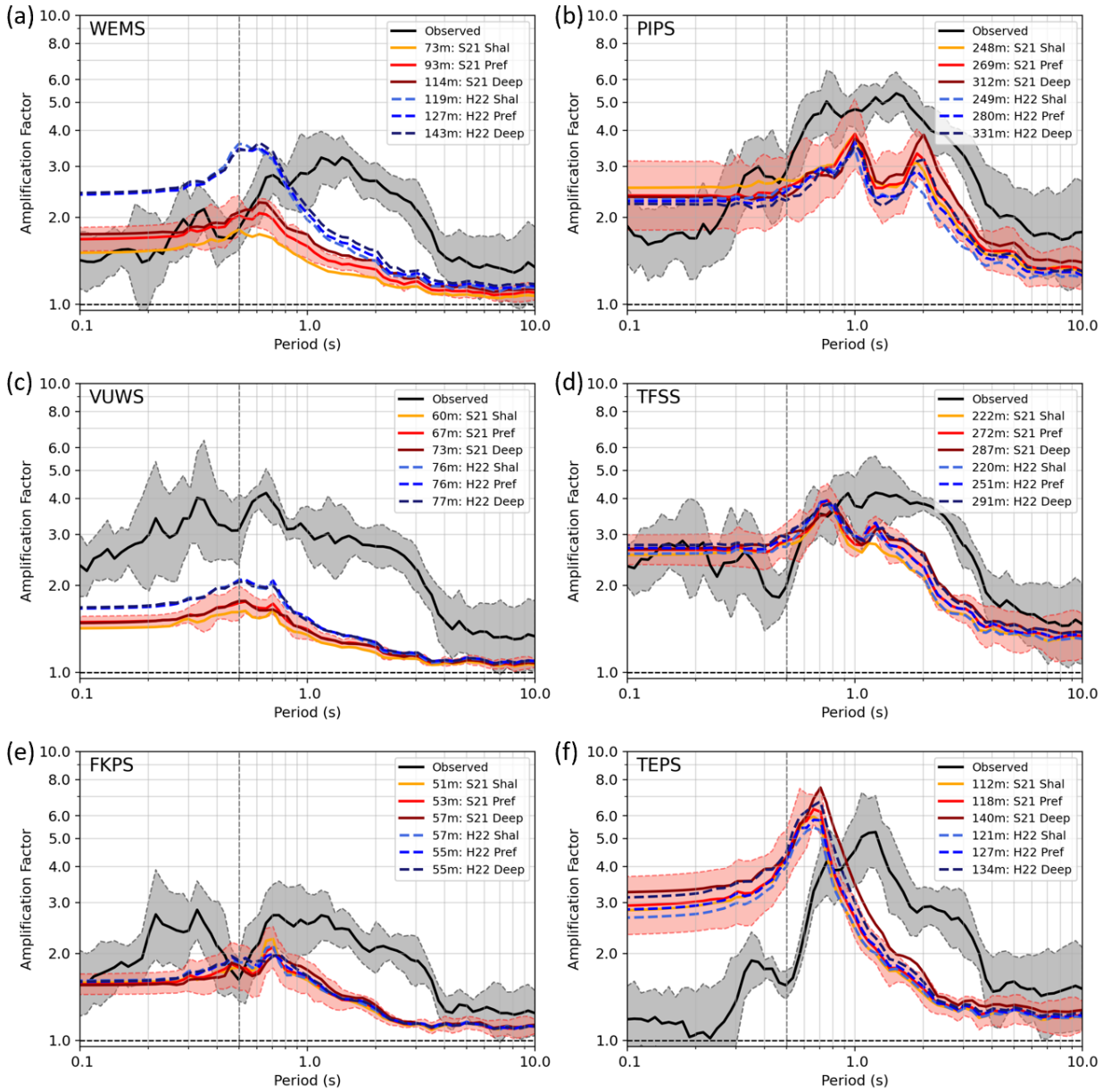

Figure 4: Simulated site amplification factors for each basin model and observed site amplification factors averaged across the 6 earthquakes for locations: (a) WEMS, (b) PIPS, (c) VUWS, (d) TFSS, (e) FKPS, and (f) TEPS. The grey and red-shaded areas indicate the +/-1 standard deviation of the observed and S21 Pref model, respectively. H21 model is not shown to mitigate visual clutter. The vertical dashed line indicates T=0.5 s which is the minimum reliable period of the LF simulations.

6 DISCUSSION AND CONCLUSIONS

This paper presented a region-specific study on site amplification related to basin effects in Wellington, NZ, predicted through 3D physics-based ground motion simulations. There were mostly minor differences in the level of amplification and period-dependent trends between basin models, except at shallow basin locations with very different depth to rock between models. Compared to observed amplification factors, the simulated amplification factors can have misaligned spectral peaks. Several limitations have been highlighted including

the need for lower minimum S-wave velocities in the simulations to better predict periods of spectral amplification peaks and higher spatial resolution in the simulations to better capture basin response at locations with shallow basin depth. At deep sites, the simulations were often able to produce comparable levels of amplification at moderate vibration periods. Further work will be required to improve the simulations to provide more accurate and stable predictions towards their consideration in routine seismic hazard analyses.

7 ACKNOWLEDGEMENTS

The authors would like to gratefully acknowledge the NZ MBIE for funding the 2022 NZ NSHM revision.

REFERENCES

Bradley BA, Wotherspoon LM, Kaiser AE, Cox B and Jeong S (2018). "Influence of site effects on observed ground motions in the Wellington region from the M_w 7.8 Kaikōura, New Zealand, Earthquake". *Bulletin of the Seismological Society of America*, **108**(3B): 1722–1735. https://doi.org/10.1785/0120170286

Graves R and Pitarka A (2016). "Kinematic ground-motion simulations on rough faults including effects of 3D stochastic velocity perturbations". *Bulletin of the Seismological Society of America*, **106**(5): 2136–2153. https://doi.org/10.1785/0120160088

Hill MP, Kaiser AE, Wotherspoon LM, Manea EF., Lee RL, de la Torre C. and Bradley BA (2022). "*3D geological modelling of wellington quaternary sediments and basin geometry*". GNS Science Consultancy Report 2022/33, GNS Science, 58pp. https://doi.org/10.21420/TS0B-8A37

Hutchinson JA, Bradley BA, Lee RL, Wotherspoon LM, Dupuis M, Schill C, Motha J, Kaiser AE and Manea EF (2022). "*2021 New Zealand ground-motion database*". GNS Science Consultancy Report 2021/56, GNS Science, 45p. https://doi.org/10.21420/Z20E-5507

Leonard M (2010). "Earthquake fault scaling: Self-consistent relating of rupture length, width, average displacement, and moment release". *Bulletin of the Seismological Society of America* **100**(5A): 1971–1988. https://doi.org/10.1785/0120090189

Stronach A and Stern T (2021). "A new basin depth map of the fault-bound Wellington CBD based on residual gravity anomalies". *New Zealand Journal of Geology and Geophysics*, **66**(1): 27-41. https://doi.org/10.1080/00288306.2021.2000438

Thomson EM, Bradley BA and Lee RL (2019). "Methodology and computational implementation of a New Zealand velocity model (NZVM2.0) for broadband ground motion simulation". *New Zealand Journal of Geology and Geophysics*, **63**(1): 110-127. https://doi.org/10.1080/00288306.2019.1636830